




Effect of Spacing and Skewness on Side-by-Side Bridge Piers

Hawra'a A. Yassin^{*}, Abdul Hassan K. Al-Shukur^{ID}

Department of Civil Engineering, Faculty of Engineering, Babylon University, Babylon 51001, Iraq

Corresponding Author Email: Hawraa.Hamood.engh328@student.uobabylon.edu.iq

Copyright: ©2025 The authors. This article is published by IETA and is licensed under the CC BY 4.0 license (<http://creativecommons.org/licenses/by/4.0/>).

<https://doi.org/10.18280/mmep.120406>

ABSTRACT

Received: 22 September 2024

Revised: 28 November 2024

Accepted: 13 December 2024

Available online: 30 April 2025

Keywords:

bridge piers, local scour, horseshoe vortex, side-by-side, pier spacing

The impact of pier shapes, spacing, skew angle, and non-uniform sediment on local scour brought on by clear-water flow around three side-by-side (rectangular and lenticular) bridge piers was investigated experimentally. The experiments varied the spacing between piers' and four different pier skew angles (0° , 30° , 45° , and 60°), the sediment has mean particle size ($d_{50}=0.873$ mm), and a flow depth of 5 cm, and $S/D_p=1$ and 3. The results show that under all flow conditions, Maximum Scour Depth (MSD) were found in front of the bridge piers, regardless of the size of the piers. Because of the extensive exposed area, the rectangular form has the largest MSD=10.6, 8.8, and 6.5 for P_1 , P_2 , and P_3 , respectively at a skew angle of 30° and $S/D_p=1$, otherwise, the lenticular shapes are the best for piers Since they reduce scour depth by 30% compared to rectangular shapes when the skew angle increased from (0° - 30°) the scour depth increased, but when the skew-angle was more than 30° the scour depth decreased for the same S/D_p . When $\alpha \geq 45^\circ$, the scour downstream increases. The scour depth decreases when the spacing increases ($\alpha=0^\circ$ and 30°). On the other hand, for the skew angle of 45° , the scour depth is greater when ($S/D_p=1$) compared to ($S/D_p=3$) when the skew angle is ($0^\circ - 30^\circ$), but when the skew angle is more than 30° , the scour depth increased as the spacing between the piers increased. Additionally, it shows the MSD decreased as the armor layer's grain size increased.

1. INTRODUCTION

Most bridge collapses globally are caused by local scour, which is probably the most common danger to bridge piers and foundations [1].

Recently, several studies have investigated the impact of different factors on the creation of vortex systems around bridge piers. These factors can be classified into three groups: (1) flow parameters, such as approach velocity and flow depth; (2) sediment parameters, including median size, size distribution, and sediment density; and (3) pier characteristics, including shape, type, and dimensions [2-7]. A significant factor that increases the scour danger of bridges is the pier geometry. The pier geometry significantly influences the development and resistance of the vortex system [1, 6, 8-12].

The vertical shape of the pier at the riverbed substantially affected the flow structure. This leads to significant variations in the flow field based on the pier shape, resulting in different scour patterns. The most important variables in the scour process are the vortices generated from the pressure differentials when the water velocity profile encounters an obstruction. The scouring mechanism occurs because of the complex vortex of a system. This system includes a horseshoe vortex, wake vortex, trailing vortex, and bow-wave vortex [12, 13].

According to the study conducted by Namaee and Sui [14], the horseshoe vortex, which is mainly caused by the

downflow, is located on the pier's upstream face. The horseshoe vortex and fast flow close to the piers increased the bed shear stress, resulting in localized scour formation around the piers. Then, the horseshoe and wake vortices gradually subsided, the scouring process decreased, and the bed shear stress decreased. Consequently, the bed shear stress exceeds the critical shear stress, causing the scour hole to reach an equilibrium state where the sediment particles are no longer transported or moved into suspension. There are two types of vortices: wake vortices caused by the separation area at the sides and downstream of the pier, and horseshoe vortices at the front side of the pier [15].

Two different situations related to sediment transport may cause scour: (1) clear water, which refers to the absence of sediment transport in the approach channel bed, and (2) live beds, which refers to the transport of bed sand in the approach flow. In the first condition, at the start of the sediment motion, the shear stress at the bed is less or, most likely, equal to the critical shear stress at the bed; in the second condition, the shear stress at the bed exceeds the critical shear stress. Localized and general scours are the two main types of scour. The combination of contraction and local scour results in localized scour rather than general scour owing to the presence of the bridge. Ignoring the local scour phenomena in the pier design may lead to a high mortality rate or significant financial loss. Sediment particle movement is related to the creation of an armor layer in the scour hole surrounding piers. As a result,

coarser grains remain behind while finer sediment particles move. The remaining finer grains are concealed by the bigger grains, and the coarser grains to greater flow [16]. Armoring is primarily caused by selective erosion, wherein the critical shear stress for movement (τ^*c) exceeds the shear stress at the bed of finer sediment particles (τ). When there is clear water flow, scour at bridge piers can take a long time to stabilize, mainly if the flow velocity is close to the threshold for the first sediment movement. This is because of the removal of the entire volume of sediment particles from the scour hole and the interaction of flowing water with the pier under the influence of vortices, which determine the equilibrium scour depth. When the scour depth is at equilibrium, it ceases to fluctuate over time [17].

Based on the literature review above, pier erosion is a complicated phenomenon that can have serious repercussions, including the whole or partial collapse of bridges. In the coming decades, there will be a significant increase in flood occurrences and unanticipated variations in river flow as a consequence of warming [18], uneven distribution of rainwater [19], caused by water pollution [20], and human activities [21]. Several studies involving deep lab tests have been conducted to examine pier scours. In most of these tests, the scour at the pier was examined under conditions of uniform sediment. Based on a review of the literature, it was discovered that there has yet to be much research done on scour surrounding side-by-side piers, and there have not been enough studies published on when sediment conditions are non-uniform and with varying spacings between side-by-side bridge piers.

2. MODEL OF THE PIERS

This study aims to employ different pier shapes (rectangular and lenticular) and skew angles $\alpha=0^\circ, 30^\circ, 45^\circ$, and 60° with specific flow conditions. The manufactured hypothetical piers with $D_p=4.5$ cm, $L=40$ cm, and $h=50$ cm. The pier models have a constant length-to-width ratio of 8.88 and a steady flow depth of $Y_o=5$ cm. According to Melville’s study [13], the pier diameter is carefully selected to avoid the impact of contraction on scour depth (reduce blockage effects, often referred to as sidewall effects) The flume width must be at least ten times the D_p . Experiments were conducted with three (rectangular and lenticular) piers arranged in one row, the piers were positioned at the flume centerline when the flow direction was vertical or angled relative to the pier alignment. Figure 1 shows the pier models for all shapes.

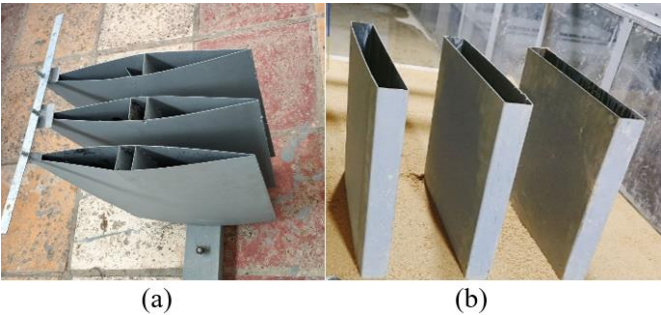


Figure 1. Pier-shape model: (a) lenticular shape and (b) rectangular shape

3. MATERIALS AND METHODS

3.1 Material of bed

The amount of natural sediment can vary greatly, depending on the geology and stream strength of the area. Sediment size is crucial because it affects sediment settling velocity and specific gravity. Particle characteristics influence the scour depth. Cohesionless sediment (i.e., non-uniform Iraqi soil) was used as the bed material for each experiment to achieve the MSD. As shown in Figure 2, a soil-grading test (sieve analysis) was performed by Arneson et al. [22] to determine the types and characteristics of the sand used in this investigation. The bed material specifications are listed in Table 1.

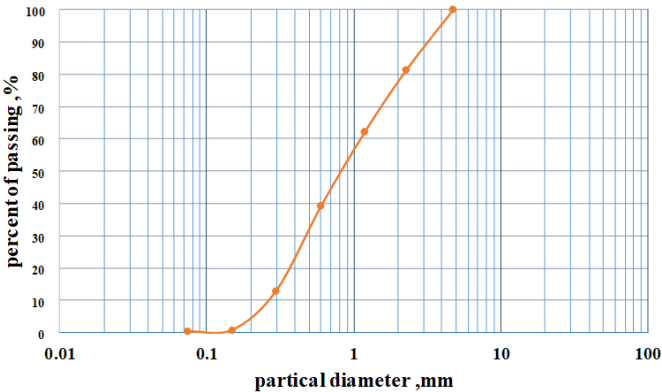


Figure 2. Distribution curves of non-uniform sediments

Table 1. The specification of bed material

Parameters	Value
d_{50}	0.873 mm
ρ	1637 kg/m ³
σ_g	2.81 > 1.3

The starting velocity of coarse particles in non-uniform materials is less than that of uniform materials with identical particle sizes, and the starting velocity of finer particles in non-uniform materials is higher than that of uniform materials with identical particle sizes, as seen in the study of Xu et al. [23]. Because coarse grains are more likely to be exposed to flow while transporting non-uniform soil, they are easier to entrain than uniform sediment particles of the same particle size.

3.2 Experimental setup and measurement

The tests were conducted at a private hydraulic laboratory in Babylon. The flume was made of a steel frame constructed with glass walls. It is horizontally non-tilting, 8.5 m long, 0.98 m wide, and 0.6 m deep. The work section was 2.1 m long and 0.204 m deep. Located 2.5 m upstream from the flume inlet section, the section has been filled with cohesion-less soil $d_{50}=0.873$ mm Additionally, water is pumped from the main reservoir tank into an overhead tank located upstream of the flume. A wooden gate suppressor was used in the upstream approach section, and baffles (two screens) were positioned every 50 cm from the flume entrance to smooth the flow (steady continuous flow) into the bed section. A rectangular gate 0.98×0.6 m was supplied at the flume outlet section to make the water depth at the head and end of the flume equal and hence to control the flow velocity. The water utilized from

the flume was then discharged into the outlet tank. The pump extracts water from the reservoir at the downstream terminus of the flume and conveys it to the upstream terminus via a 4-inch-diameter pipeline that runs parallel to the flume. Four reservoir tanks exist, one located in the outflow flume with dimensions 1×0.98×0.55 m, separated by a rectangular gate, and three parallel to the flume with a size 1.25×1.25×0.5 m. A centrifugal pump positioned at the end of the downstream of the flume delivered the flow rate via a 3-inch-diameter pipe. An ultrasonic flow meter was employed to quantify the water discharge, and all depths were gauged using a movable point gauge affixed to a brass rail at the upper section of the flume side with an accuracy of - 0.1 mm, as shown in Figure 3.

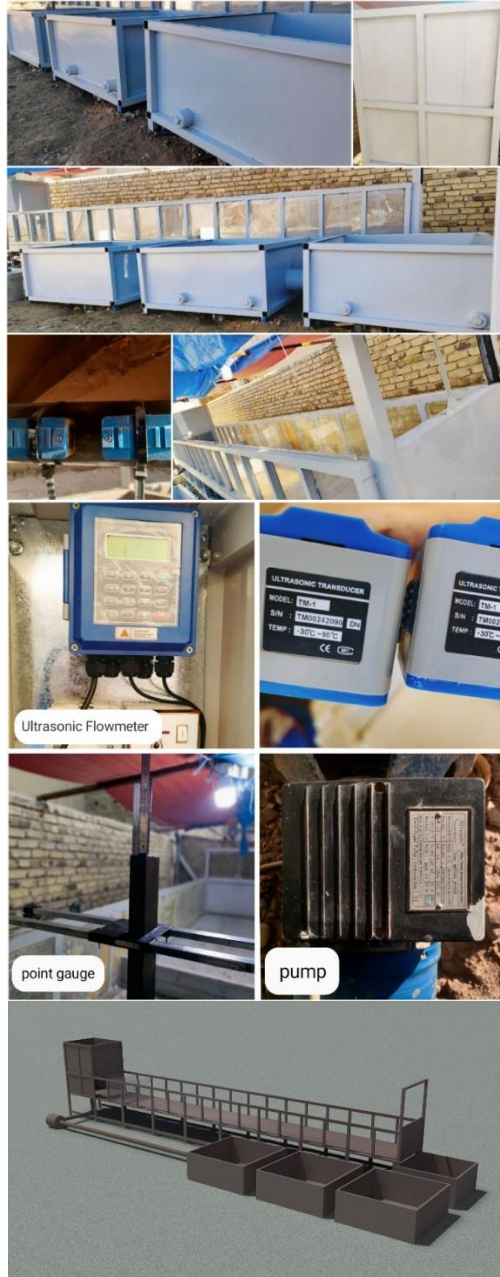


Figure 3. The experimental flume

3.3 General experiment procedures

1. The models were installed at the required spacing and skew angles (vertically or skew angles). Changes in pier position and direction may significantly affect the flow pattern.

2. The bed material, consisting of sand with a mean grain size $d_{50}=0.873$ mm, was positioned in the work section. The sand was leveled using a scraper, and the initial bed elevations were verified at random spots using a point gauge to ensure proper leveling. The sand layer had a thickness of 20.4 cm.

3. The gate is closed downstream. The pump started operating, and its speed was gradually increased until the required flow rate was attained. The tailgate was verified to preserve the correct flow depth of the flume.

4. The timer recorded the time during each test. When the time limit ended, the flow stopped and the flume was gradually emptied to prevent the scour hole from changing.

5. After the sand was left to dry, the positions and sizes of the MSD points were recorded. During the initial hours, data on the MSD were recorded every few minutes. The initial hours of every test are critical because many readings are required to correctly determine the early stage of the maximum scour depth vs. time graph.

6. After changing the skew angle, pier shape, and pier spacing, the sand was leveled again and the processes were repeated.

3.4 Scour conditions

In the series of tests, fourteen experiments were shown in terms of flow skew-angle $\alpha=0^\circ, 30^\circ, 45^\circ, 60^\circ$, the corresponding steady discharge was 12.5 lit/sec, approach velocity, V , critical velocity, V_c , Armor peak velocity are valid only for $\sigma_g > 1.3$ (non-uniform sediments), V_a , flow density, $([V - (V_a - V_c)]) / V_c < 1$ for non-uniform sediments, clear water scours conditions are present, maximum scour depth, ds , and Froude number, $Fr < 1$ (subcritical for all cases), with soil (sand $d_{50} = 0.873$ mm, $d_{50a} = 1.267$ mm), and approach flow depth $Y_o=0.05$ m, pier diameter (D_p), and pier spacing (S).

$$d_{50a} = \frac{d_{max}}{1.8}$$

d_{max} = maximum particle size

The critical shear velocities in the armored beds were obtained from Eqs. (1) and (2) [13]:

$$0.1\text{mm} < d_{50a} < 1\text{ mm} \quad V_{*ca} = 0.0115 + 0.0125 d_{50a}^{1.4} \quad (1)$$

$$1\text{ mm} < d_{50a} < 100\text{ mm} \quad V_{*ca} = 0.0305 d_{50a}^{0.5} - 0.0065 d_{50a}^{-1} \quad (2)$$

The mean critical velocity on the armored bed was:

$$\frac{V_c}{V * ca} = 5.75 \log \left[5.53 \frac{Y_o}{d_{50a}} \right] \quad (3)$$

V_{*ca} : mean critical velocity in armored bed.

Finally, $V_a = 0.8 V_{*ca}$.

$$\frac{[V - (V_a - V_c)]}{V_c} < 1 \text{ (for non-uniform sediment)} \quad (4)$$

Then $Q = VA$.

4. RESULTS AND DISCUSSION

The impact of non-uniform bed material, pier shape, and pier spacing on the scour development around three side-by-

side pier arrangements was studied in the laboratory. The experimental results describe the scour patterns around three (rectangular and lenticular) side-by-side bridge piers arranged in one row of 45 mm width, with the spacing ratio between piers to the width pier ($S/D_p=1$ and 3). After twenty-four hours of continuous operation, the point of the MSD is situated directly in front of the piers.

Figure 4 shows the rectangular and lenticular side-by-side bridge pier spacing ratio ($S/D_p=1$) with three side-by-side piers arranged vertically in the flow direction ($\alpha=0^\circ$).



Figure 4. Experimental details when ($S/D_p=1$ and $\alpha=0^\circ$) for (a) rectangular piers and (b) lenticular piers

Because of the large exposed area for a rectangular shape, the point of the MSD is always directly in front of the piers and extends approximately 2/3 of the piers from the upstream side. The middle pier (P_2) had a lower MSD than the side piers, whereas the MSDs at the P_1 and P_3 bridge piers were almost equal, and each pier had a unique scour hole. The representation of scour depth variation with time shows that scour development stops after only 150 min, as shown in Figure 5.

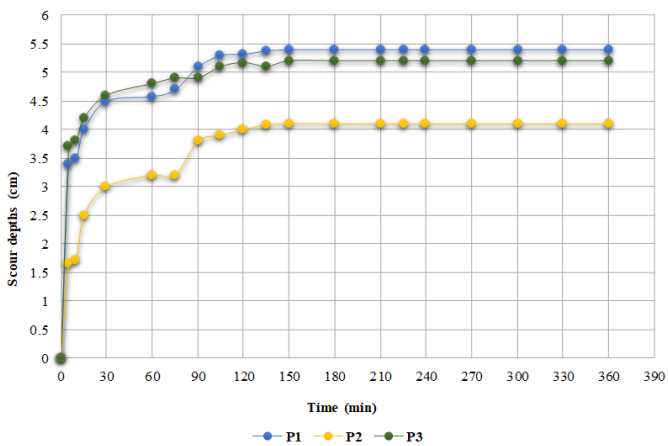


Figure 5. Scour depth development with time for rectangular piers ($\alpha=0^\circ$ and $S/D_p=1$)

The results of the lenticular experiment show that the scour depth patterns are the same for rectangular shapes when ($S/D_p=1$), and the piers had a scour-like one-hole approximately.

The representation of the scour depth variation with time ensures that the scour development stops after 210 min, as shown in Figure 6.

Figure 7 shows the rectangular and lenticular side-by-side bridge-pier spacing ratios ($S/D_p=3$ and $\alpha=0^\circ$).

Figure 8 shows the time-varying development of scour depth at the scour depth for rectangular and lenticular shapes. For each pier shape, the scour depth initially grew, attaining a

maximum value, and subsequently approached observations indicate that approximately 75% of the maximum scour depth had been achieved within the initial three hours of the experiment.

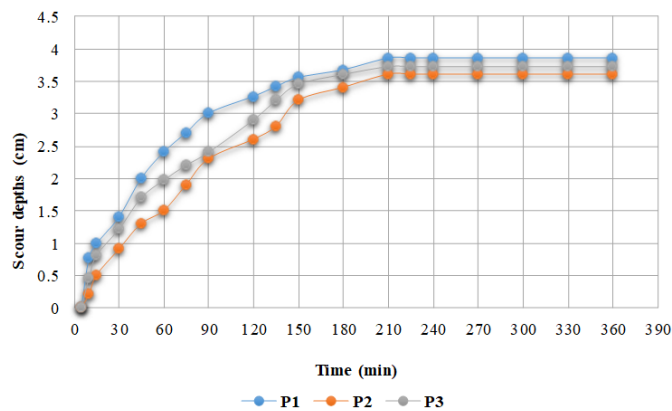


Figure 6. Scour depth development over time for lenticular piers ($\alpha=0^\circ$ and $S/D_p=1$)

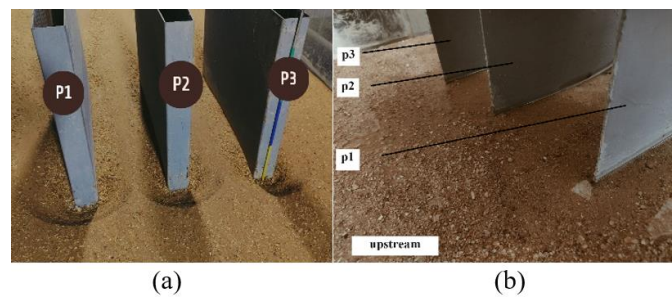


Figure 7. Experimental details when ($S/D_p=3$ and $\alpha=0^\circ$) for (a) rectangular piers and (b) lenticular piers

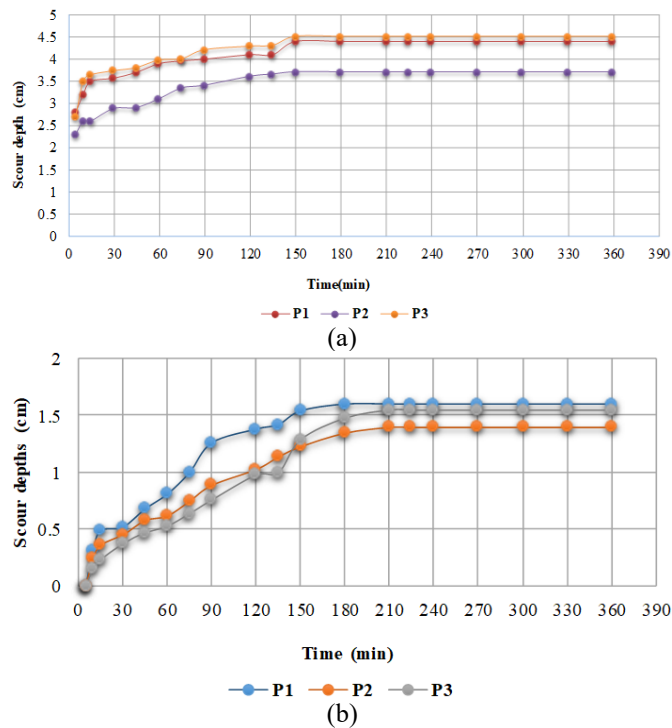


Figure 8. Scour depth variation with time when ($\alpha=0^\circ$ and $S/D_p=3$) for (a) rectangular and (b) lenticular piers

The results show the same scour depth pattern of ($S/D_p=1$). The scour depth when ($S/D_p=1$) is large compared to ($S/D_p=3$),

which means that when S/D_p decreases, the scour depths increase owing to the blockage resulting from sediments between the side-by-side bridge piers, which causes difficulty in transporting the sediments; therefore, the side-by-side bridge piers act as one pier, which means an increase in the exposed area that intercepts the flow, which results in a greater scour depth, and the scour is like a hole.

The geometry of the lenticular piers significantly reduces the formation of a horseshoe, wake vortices are generated, and subsequently minimizes the scour depth, which may be the reason why lenticular piers performed better in terms of scour depth than rectangular piers [24].

Figure 9 shows the effects of the skewness angles (30° , 45° , and 60°) on the rectangular and lenticular side-by-side bridge pier spacing ratios ($S/D_p=1$).

The maximum scour depth for (30° , 45° , and 60°) was found near the flume wall in the P_1 , P_2 , and P_3 corners, respectively, owing to the short distance between P_1 and the sidewall of the flume, and the piers had a roughly scour-like one-hole. The maximum scour depths were found along the entire upstream region from the P_1 side. The time-varying development of scour depth at the position of scour depth for rectangular and lenticular shapes. For skew angles of 30° , 45° , and 60° for each pier shape, approximately 95% of the maximum scour depth was achieved within 180 min. As shown in Figures 10-12.

The data obtained, shown in Figure 13, indicate that the scour depth increases when (α) increases from 0° to 30° . For the same S/D_p ratio, the scour depth decreased from 30° to 60° . Figure 13 compares MSD and (α) when $S/D_p=1$.

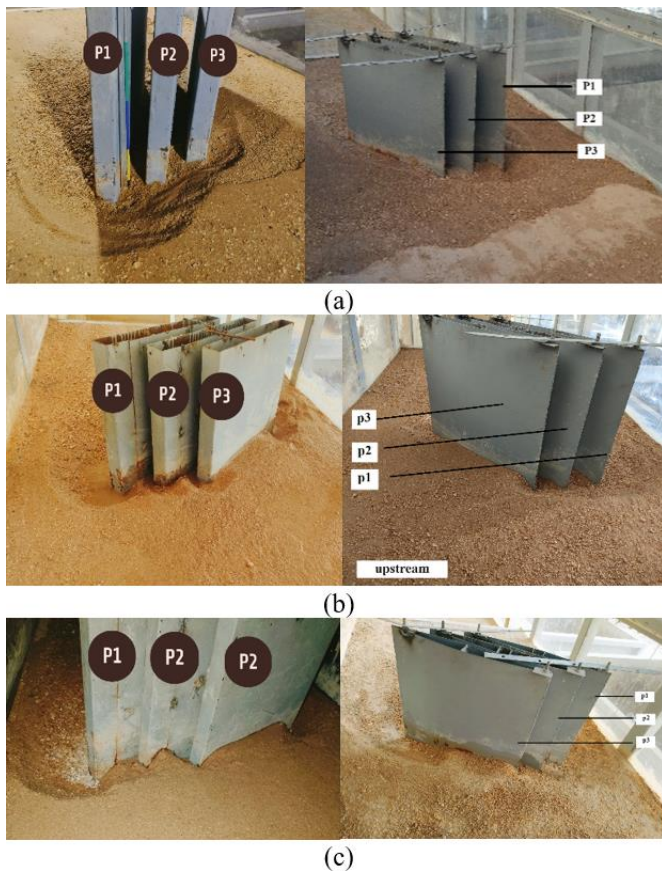


Figure 9. The experiment details the rectangular and lenticular shapes for (a) when $S/D_p=1$, and $\alpha=30^\circ$ (b) when $S/D_p=1$, and $\alpha=45^\circ$ (c) when $S/D_p=1$, and $\alpha=60^\circ$

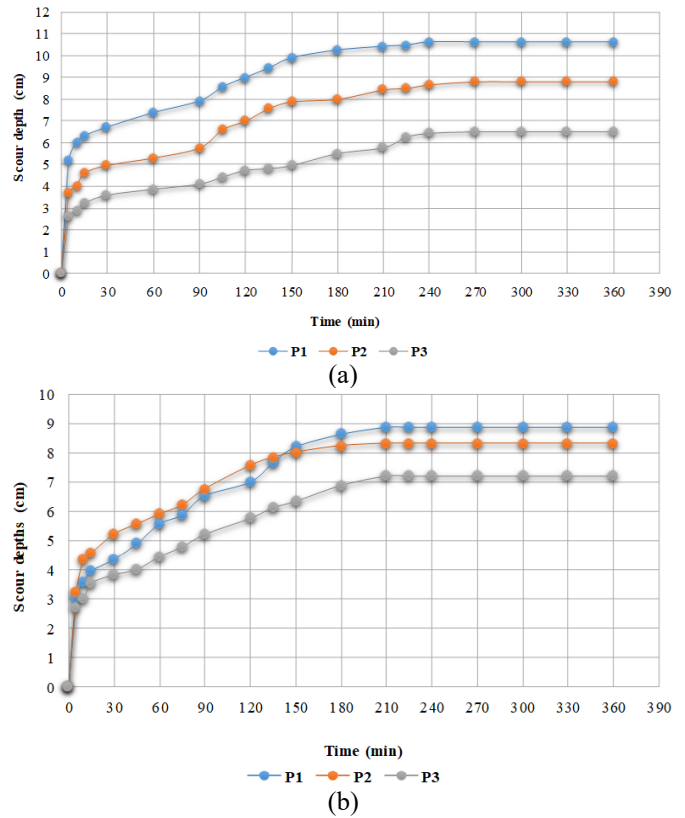


Figure 10. Scour depth development with time when $\alpha=30^\circ$ and $S/D_p=1$ for (a) rectangular and (b) lenticular piers

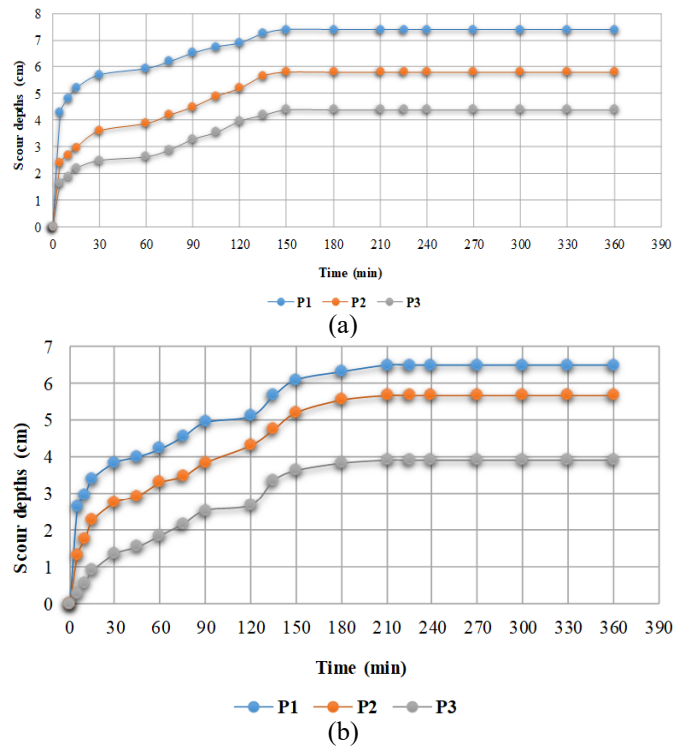


Figure 11. Scour depth development with time when $\alpha=45^\circ$ and $S/D_p=1$ for (a) rectangular and (b) lenticular piers

Figure 14 shows the effects of the skewness angles 30° and 45° when the pier spacing ratio $S/D_p=3$ was used.

MSD is located in the P_1 , P_2 , and P_3 corners near the flume wall; however, it has a smaller MSD from $S/D_p=1$, and each pier has its own scour hole approximately, and MSD occurs along the whole upstream from the side of P_1 . The time-

varying development of scour depth at the position of scour depth for rectangular and lenticular shapes. For skew angles of 30° and 45° with $S/D_p=3$ for each pier shape, the equilibrium scour depth was reached at 180 min, as shown in Figures 15 and 16.

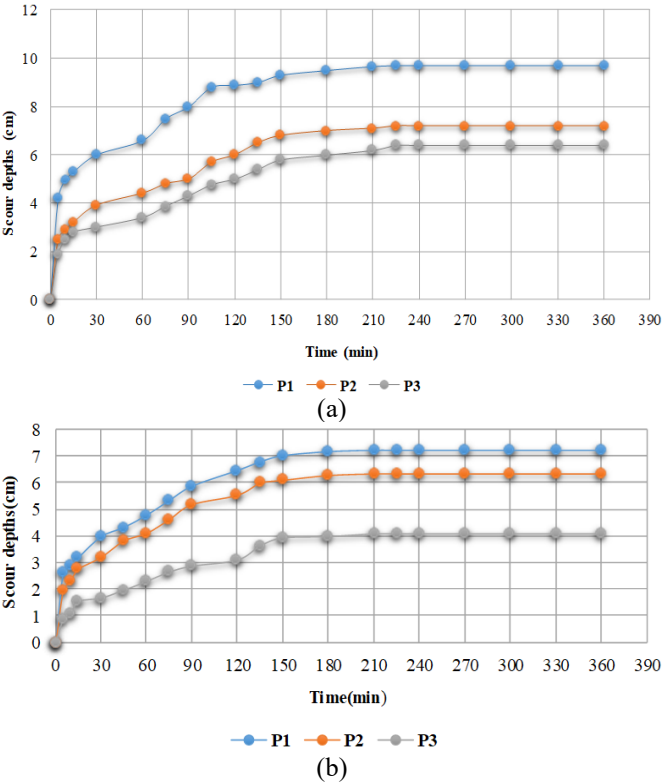


Figure 12. Scour depth development with time when $\alpha=60^\circ$ and $S/D_p=1$ for (a) rectangular and (b) lenticular piers

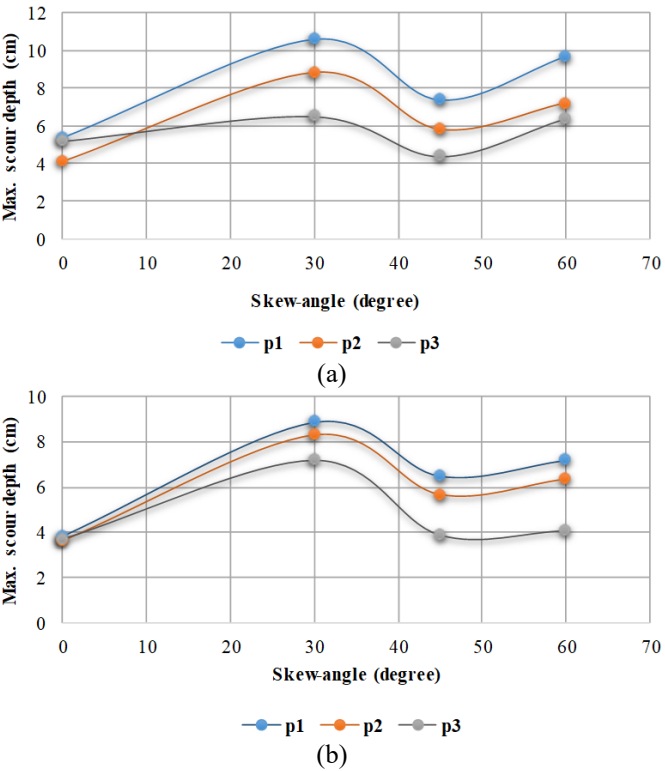


Figure 13. Comparison between MSD and skewness angle when $S/D_p=1$ for (a) rectangular piers and (b) lenticular piers

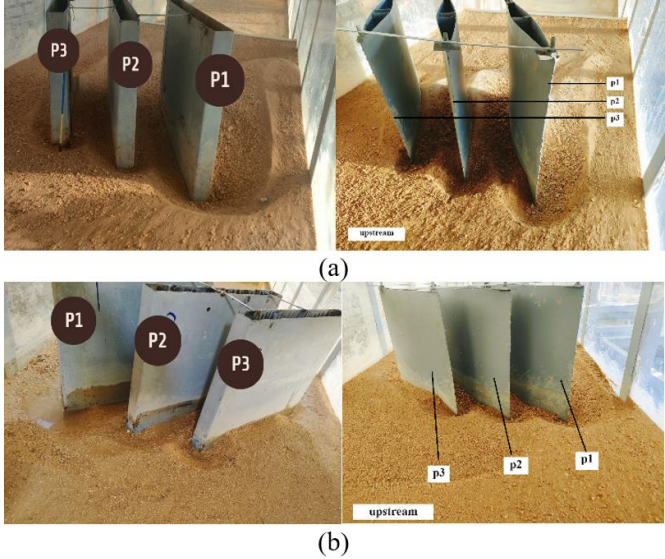


Figure 14. The experiment details the rectangular and lenticular shapes for (a) when $S/D_p=3$, and $\alpha=30^\circ$ (b) when $S/D_p=3$, and $\alpha=45^\circ$

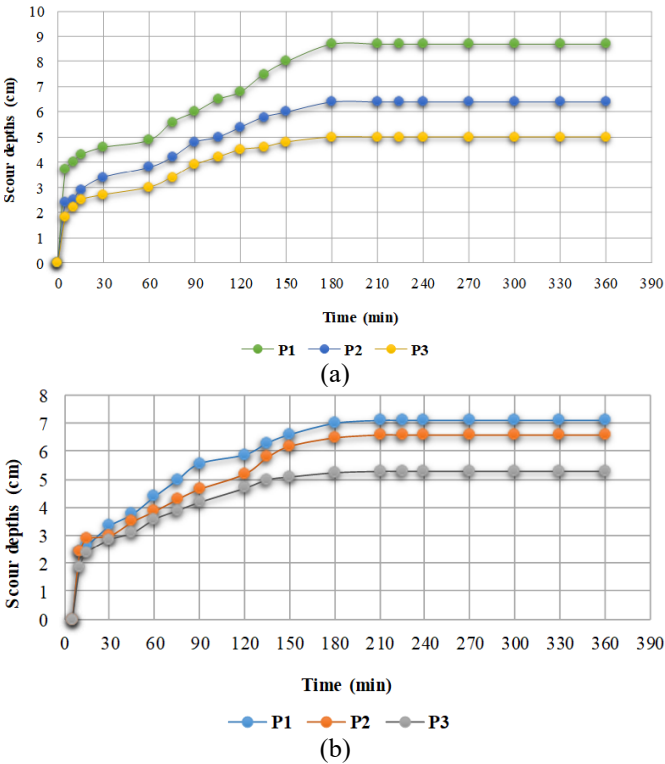
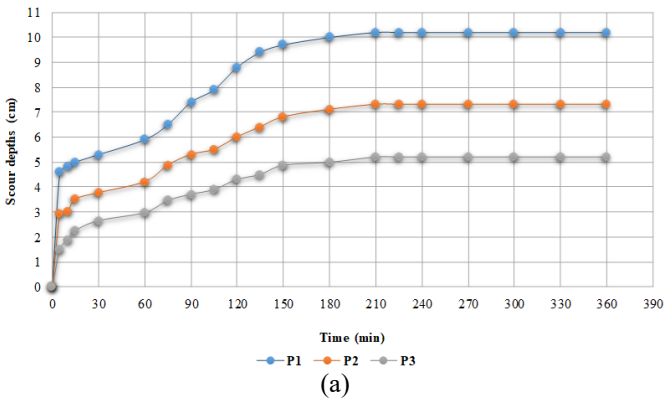


Figure 15. Scour depth development with time when $\alpha=30^\circ$ and $S/D_p=3$ for (a) rectangular and (b) lenticular piers



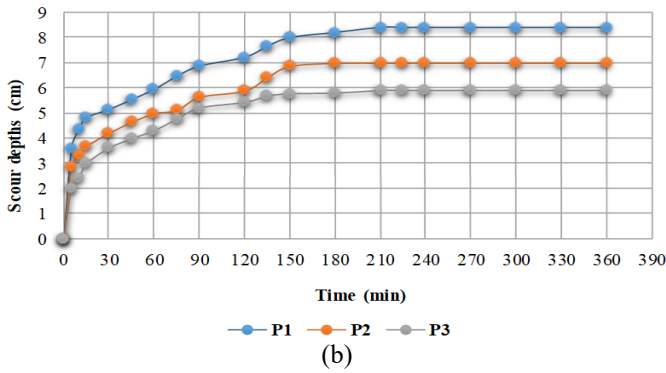


Figure 16. Scour depth development with time when $\alpha=45^\circ$ and $S/D_p=3$ for (a) rectangular and (b) lenticular piers

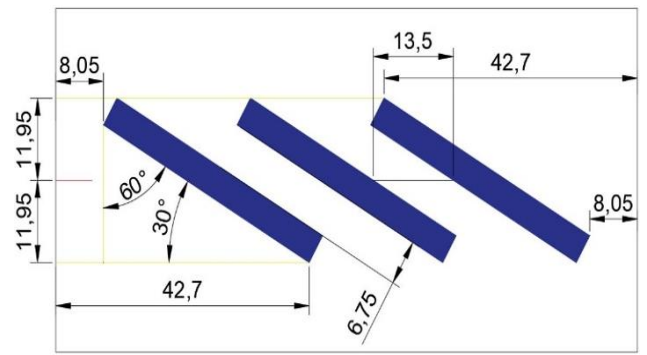


Figure 17. Spacing ratio for rectangular side-by-side bridge piers when $S/D_p=3$ and $\alpha=60^\circ$

Table 2. A summary of the series of experimental data

Run	Pier-Shape	α°	Q (l/s)	Y _o (m)	S/D _p	V (m/s)	V _c (m/s)	V _a	$\frac{([V - (V_a - V_c)])}{V_c}$	Max. Scour Depth (cm)			F _r
										P ₁	P ₂	P ₃	
1	Rectangular	0°	12.5	0.05	1	0.258	0.392	0.314	0.85	5.4	4.1	5.2	0.364
2	Rectangular	0°	12.5	0.05	3	0.258	0.392	0.314	0.85	4.4	3.7	4.2	0.364
3	Rectangular	30°	12.5	0.05	1	0.258	0.392	0.314	0.85	10.6	8.8	6.5	0.364
4	Rectangular	30°	12.5	0.05	3	0.258	0.392	0.314	0.85	8.7	6.4	5	0.364
5	Rectangular	45°	12.5	0.05	1	0.258	0.392	0.314	0.85	7.4	5.8	4.4	0.364
6	Rectangular	45°	12.5	0.05	3	0.258	0.392	0.314	0.85	10.2	7.3	5.2	0.364
7	Rectangular	60°	12.5	0.05	1	0.258	0.392	0.314	0.85	9.7	7.2	6.4	0.364
8	Lenticular	0°	12.5	0.05	1	0.258	0.392	0.314	0.85	3.85	3.6	3.72	0.364
9	Lenticular	0°	12.5	0.05	3	0.258	0.392	0.314	0.85	1.6	1.4	1.55	0.364
10	Lenticular	30°	12.5	0.05	1	0.258	0.392	0.314	0.85	8.87	8.3	7.2	0.364
11	Lenticular	30°	12.5	0.05	3	0.258	0.392	0.314	0.85	7.1	6.6	5.3	0.364
12	Lenticular	45°	12.5	0.05	1	0.258	0.392	0.314	0.85	6.5	5.66	3.9	0.364
13	Lenticular	45°	12.5	0.05	3	0.258	0.392	0.314	0.85	8.4	7	5.9	0.364
14	Lenticular	60°	12.5	0.05	1	0.258	0.392	0.314	0.85	7.2	6.35	4.1	0.364

$\alpha=45^\circ$ shows the opposite for $\alpha=0^\circ$, and 30° , where the scour depth is greater when ($S/D_p=3$) than ($S/D_p=1$), when $\alpha=45^\circ$, the flow fails to move the sediment between the piers due to the more skewness, resulting in a blockage, the exposed area to the flow when $S/D_p=3$ is greater than $S/D_p=1$, and the spacing between the pier and sidewall is smaller when $S/D_p=3$ than $S/D_p=1$, and ($\alpha=60^\circ$) shows the same pattern.

However, the experiment could not be carried out for a skew angle of 60° when ($S/D_p=3$) because it did not meet the criteria owing to the spacing between the pier and sidewall (referred to as sidewall effects), as shown in Figure 17.

The data showed that the rectangular piers experienced the greatest scour depth (10.6, 8.8, 6.5) cm for P₁, P₂, and P₃, respectively, at ($\alpha=30^\circ$ and $S/D_p=1$). Numerous earlier studies have produced comparable findings [25].

Table 2 shows that the lenticular pier was the most resistant to local scour. All the investigated parameters had a considerable impact on the scour depth, according to the obtained data. It has also been discovered that by using lenticular piers and maintaining the flow intensity, the scour depth can be reduced. In summary, the results showed that each parameter under study had a considerable impact on scour depth.

5. CONCLUSION

Fourteen experiments were conducted to investigate the local scour pattern in a horizontal open channel under clear water flow conditions utilizing different shapes, skew angles,

and spacing between piers around three side-by-side rectangular and lenticular bridge piers.

1. At the beginning of each run, the rate of scour hole creation was larger; it then decreased with time and asymptotically approached an equilibrium value, with a maximum period of approximately 180-210 minutes. The maximum equilibrium scour depth of a clear-water local scour is a function of the relative size D_p/d_{50} , relative depth Y_o/D_p , and spacing ratio S/D_p , and the MSD occurs at the pier near the abutment upstream in all experiments.

2. The pier shape and skew angle influenced the initial scour rate and equilibrium scour depth. The maximum scour from the upstream side of the pier is approximately two-thirds of its length.

3. For lenticular pier when $\alpha=0^\circ$ and $S/D_p=3$, the lowest scour observed with the scour depths are 1.6, 1.4, and 1.55 cm for P₁, P₂, and P₃, respectively because its geometry is assumed to be the most efficient protective measure against horseshoe vortices which cause local scour; the scour starts merely from the upstream face and ends at mid-section, it is the best compared to rectangular piers, and the MSD scour hole is identified at $\alpha=30^\circ$ and $S/D_p=1$, with scour depths measuring 8.87, 8.3, and 7.2 cm for P₁, P₂, and P₃, respectively.

4. A rectangular pier has a higher scour than other geometries because of the maximum exposed area, in which the deepest MSD scour hole is observed for $\alpha=30^\circ$, and $S/D_p=1$ for the rectangular pier scour depths are 10.6, 8.8, and 6.5 cm for P₁, P₂, and P₃, respectively, the rectangular pier is regarded as the weakest pier shape.

5. Smaller scour depths were obtained when the skew

angle was 0° . Based on the scour profiles, the skew angle is in control of both horizontal expansion (the length increases in the direction of the transverse axis of the pier cross-section) and vertical deepening of the scour hole around the pier, in addition to the longitudinal deposition of sand downstream, as found in the study [26].

6. For $\alpha=0^\circ$, the scour depth decreases when the spacing increases. Previous studies confirm this, and $\alpha=30^\circ$ shows the same pattern, but $\alpha=45^\circ$ shows the opposite, where the scour depth is greater when $S/D_p=3$ than when $S/D_p=1$, because of the blockage caused by sediments between the piers, which makes it harder to transport the sediments and increases the exposed area that intercepts the flow; additionally, decreasing the spacing between the pier and abutment upstream, thereby increasing the velocity. Accordingly, the strength of the vortex increased, and the shear stress increased, thus increasing the sediment transport and hole depth.

7. According to the results, the maximum scour depth decreases as the grain size of the armor layer increases. The literature revealed Similar findings have been previously reported [27].

REFERENCES

- [1] Vijayasree, B.A., Eldho, T.I., Mazumder, B.S., Ahmad, N. (2019). Influence of bridge pier shape on flow field and scour geometry. *International Journal of River Basin Management*, 17(1): 109-129. <https://doi.org/10.1080/15715124.2017.1394315>
- [2] Salamatian, S.A., Zarrati, A.R. (2021). Reliability study on uncertainty parameters and flood duration on scouring around unprotected and protected bridge piers. *ISH Journal of Hydraulic Engineering*, 27(sup1): 11-19. <https://doi.org/10.1080/09715010.2019.1570360>
- [3] Zarrati, A.R., Nazariha, M., Mashahir, M.B. (2006). Reduction of local scour in the vicinity of bridge pier groups using collars and riprap. *Journal of Hydraulic Engineering*, 132(2): 154-162. [https://doi.org/10.1061/\(ASCE\)0733-9429\(2006\)132:2\(154\)](https://doi.org/10.1061/(ASCE)0733-9429(2006)132:2(154))
- [4] Singh, U.K., Ahmad, Z., Kumar, A. (2017). Turbulence characteristics of flow over the degraded cohesive bed of clay-silt-sand mixture. *ISH Journal of Hydraulic Engineering*, 23(3): 308-318. <https://doi.org/10.1080/09715010.2017.1313144>
- [5] Pandey, M., Ahmad, Z., Sharma, P.K. (2015). Flow-characteristics around circular pier model. *Proceedings of the HYDRO*, p. 15.
- [6] Melville, B.W. (1997). Pier and abutment scour: Integrated approach. *Journal of hydraulic Engineering*, 123(2): 125-136. [https://doi.org/10.1061/\(ASCE\)0733-9429\(1997\)123:2\(125\)](https://doi.org/10.1061/(ASCE)0733-9429(1997)123:2(125))
- [7] Melville, B.W. (1984). Live-bed scour at bridge piers. *Journal of Hydraulic Engineering*, 110(9): 1234-1247. [https://doi.org/10.1061/\(ASCE\)0733-9429\(1984\)110:9\(1234\)](https://doi.org/10.1061/(ASCE)0733-9429(1984)110:9(1234))
- [8] Dargahi, B. (1990). Controlling mechanism of local scouring. *Journal of Hydraulic Engineering*, 116(10): 1197-1214. [https://doi.org/10.1061/\(ASCE\)0733-9429\(1990\)116:10\(1197\)](https://doi.org/10.1061/(ASCE)0733-9429(1990)116:10(1197))
- [9] Yanmaz, A.M., Ustun, I. (2001). Generalized reliability model for local scour around bridge piers of various shapes. *Turkish Journal of Engineering and Environmental Sciences*, 25(6): 687-698.
- [10] Zarrati, A.R., Gholami, H., Mashahir, M.B. (2004). Application of collar to control scouring around rectangular bridge piers. *Journal of Hydraulic Research*, 42(1): 97-103. <https://doi.org/10.1080/00221686.2004.9641188>
- [11] Fael, C., Lança, R., Cardoso, A. (2016). Effect of pier shape and pier alignment on the equilibrium scour depth at single piers. *International Journal of Sediment Research*, 31(3): 244-250. <https://doi.org/10.1016/j.ijsrc.2016.04.001>
- [12] Lee, C.H., Xu, C., Huang, Z. (2019). A three-phase flow simulation of local scour caused by a submerged wall jet with a water-air interface. *Advances in Water Resources*, 129: 373-384. <https://doi.org/10.1016/j.advwatres.2017.07.017>
- [13] Melville, B.W. (2000). *Bridge Scour*. Water Resources Publications, Highlands Ranch, USA.
- [14] Namaee, M.R., Sui, J. (2020). Velocity profiles and turbulence intensities around side-by-side bridge piers under ice-covered flow condition. *Journal of Hydrology and Hydromechanics*, 68(1): 70-82. <https://doi.org/10.2478/johh-2019-0029>
- [15] Karimae, T.M., Zarrati, A.R. (2012). Effect of collar on time development and extent of scour hole around cylindrical bridge piers. *International Journal of Engineering*, 25(1(C)): 11-17. <https://doi.org/10.5829/idosi.ije.2012.25.01c.02>
- [16] Mao, L., Cooper, J.R., Frostick, L.E. (2011). Grain size and topographical differences between static and mobile armour layers. *Earth Surface Processes and Landforms*, 36(10): 1321-1334. <https://doi.org/10.1002/esp.2156>
- [17] Yang, Y., Melville, B.W., Macky, G.H., Shamseldin, A.Y. (2020). Temporal evolution of clear-water local scour at aligned and skewed complex bridge piers. *Journal of Hydraulic Engineering*, 146(4): 04020026. [https://doi.org/10.1061/\(ASCE\)HY.1943-7900.0001732](https://doi.org/10.1061/(ASCE)HY.1943-7900.0001732)
- [18] Hashim, K.S., Ali, S.S.M., AlRifaie, J.K., Kot, P., Shaw, A., Al Khaddar, R., Idowu, I., Gkantou, M. (2020). *Escherichia coli* inactivation using a hybrid ultrasonic—Electrocoagulation reactor. *Chemosphere*, 247: 125868. <https://doi.org/10.1016/j.chemosphere.2020.125868>
- [19] Zanki, A.K., Mohammad, F.H., Hashim, K.S., Muradov, M., Kot, P., Kareem, M.M., Abdulhadi, B. (2020). Removal of organic matter from water using ultrasonic-assisted electrocoagulation method. *IOP Conference Series: Materials Science and Engineering*, 888(1): 012033. <https://doi.org/10.1088/1757-899X/888/1/012033>
- [20] Alhendal, M., Nasir, M.J., Hashim, K.S., Amoako-Attah, J., Al-Faluji, D., Muradov, M., Kot, P., Abdulhadi, B. (2020). Cost-effective hybrid filter for remediation of water from fluoride. *IOP Conference Series: Materials Science and Engineering*, 888(1): 012038. <https://doi.org/10.1088/1757-899X/888/1/012038>
- [21] Hashim, K.S., Adeola Idowu, I., Jasim, N., Al Khaddar, R., Shaw, A., Phipps, D., Kot, P., Ortoneda Pedrola, M., Alattabi, A.W., Abdulredha, M., Alwash, R., Teng, K.H., Joshi, K.H., Hashim Aljefery, M. (2018). Removal of phosphate from river water using a new baffle plates electrochemical reactor. *MethodsX*, 5: 1413-1418. <https://doi.org/10.1016/j.mex.2018.10.024>
- [22] Arneson, L.A., Zevenbergen, L.W., Lagasse, P.F., Clopper, P.E. (2012). *Hydraulic engineering circular No.*

- 18: Evaluating scour at bridges. US Department of Transportation.
- [23] Xu, H.T., Lu, J.Y., Liu, X.B. (2008). Non-uniform sediment incipient velocity. *International Journal of Sediment Research*, 23(1): 69-75. [https://doi.org/10.1016/S1001-6279\(08\)60006-2](https://doi.org/10.1016/S1001-6279(08)60006-2)
- [24] Helmy, A., Ali, M., Ahmed, H. (2017). An experimental study of local scour around piers in the curved channels. *Journal of Multidisciplinary Engineering Science and Technology*, 4(1): 6448-6453. <https://www.jmest.org/wp-content/uploads/JMESTN42351988.pdf>.
- [25] Al-Shukur, A.H.K., Hussein, N.S. (2021). Effects of shape and skew-angle of bridge piers on local scour. *Journal of Engineering Science and Technology*, 16(3): 2748-2762.
- [26] Ahmad, N., Melville, B., Mohammad, T., Ali, F., Yusuf, B. (2017). Clear-water scour at long skewed bridge piers. *Journal of the Chinese Institute of Engineers*, 40(1): 10-18. <https://doi.org/10.1080/02533839.2016.1259021>
- [27] Namaee, M.R., Sui, J., Wu, P. (2019). Experimental study of local scour around side-by-side bridge piers under ice-covered flow conditions. *Current Practice in*

Fluvial Geomorphology-Dynamics and Diversity. IntechOpen. <https://doi.org/10.5772/intechopen.86369>

NOMENCLATURE

α	Pier alignment angle (Skew angle)
d_{50}	Mean particle size
d_{50a}	Armor peak mean particle size
D_p	Pier diameter
d_s	Scour depth
F_r	Froude number
h	Pier height
L	Pier length
Q	Flow discharge
S	Pier spacing
V	Mean flow velocity
V_a	Armor peak velocity
V_c	Critical velocity
Y_o	Approach flow depth
ρ	Density
σ_g	Geometric standard deviation